



# Composite Cellularized Structures Created from an Interpenetrating Polymer Network Hydrogel Reinforced by a 3D Woven Scaffold

Kristen L. Moffat, Kelsey Goon, Franklin T. Moutos, Bradley T. Estes, Sara J. Oswald, Xuanhe Zhao, and Farshid Guilak\*

Biomaterial scaffolds play multiple roles in cartilage tissue engineering, including controlling architecture of newly formed tissue while facilitating growth of embedded cells and simultaneously providing functional properties to withstand the mechanical environment within the native joint. In particular, hydrogels—with high water content and desirable transport properties—while highly conducive to chondrogenesis, often lack functional mechanical properties. In this regard, interpenetrating polymer network (IPN) hydrogels can provide mechanical toughness greatly exceeding that of individual components; however, many IPN materials are not biocompatible for cell encapsulation. In this study, an agarose and poly(ethylene) glycol IPN hydrogel is seeded with human mesenchymal stem cells (MSCs). Results show high viability of MSCs within the IPN hydrogel, with improved mechanical properties compared to constructs comprised of individual components. These properties are further strengthened by integrating the hydrogel with a 3D woven structure. The resulting fiber-reinforced hydrogels display functional macroscopic mechanical properties mimicking those of native articular cartilage, while providing a local microenvironment that supports cellular viability and function. These findings suggest that a fiber-reinforced IPN hydrogel can support stem cell chondrogenesis while allowing for significantly enhanced, complex mechanical properties at multiple scales as compared to individual hydrogel or fiber components.

## 1. Introduction

Adult articular cartilage is an avascular, aneural tissue, with a limited capacity for intrinsic repair. Tissue engineering seeks to combine novel technologies in cell isolation and sourcing, biomaterials, growth factors, and bioreactors to promote cartilage repair or replacement.<sup>[1]</sup> However, few cell-based repair procedures for articular cartilage show long-term improvement of efficacy over microfracture.<sup>[2]</sup> Although clinical outcomes generally have been reported as good to excellent, several complications have been reported.<sup>[3]</sup> These include overgrowth of the graft, which may be related to the lack of a biomaterial scaffold to guide tissue growth, and inadequate expansion potential without dedifferentiation of primary chondrocytes isolated from native articular cartilage.<sup>[4]</sup> Alternative cell types, including bone marrow (mesenchymal stem cells [MSCs]) and adipose derived stem cells (ASCs), also have been the subject of extensive research for cartilage tissue engineering.<sup>[5]</sup>

Historically, constructs designed for articular cartilage repair have focused


on combining cells and bioactive molecules (e.g., growth factors, cytokines, or DNA fragments) with a biomaterial scaffold whose primary function is to control the shape of the newly formed tissue, while simultaneously facilitating the attachment, proliferation, and differentiation of embedded cells.<sup>[6]</sup> A number of different scaffold materials and structures have been used for cartilage repair,<sup>[7]</sup> with many focusing on the potential of hydrogels for supporting chondrogenesis due to their high water content and transport properties.<sup>[8]</sup> In addition to influencing the growth, differentiation, and metabolic activity of encapsulated cells, scaffolds must also be capable of withstanding the mechanical environment of the native tissue that is to be replaced.<sup>[1]</sup> For example, standard single-network hydrogels (e.g., agarose, alginate, polyethylene glycol, etc.) can provide an environment that is conducive to chondrogenesis and tissue accumulation, but generally lack the mechanical integrity to withstand loading in vivo until substantial tissue growth has occurred.<sup>[9]</sup>

Dr. K. Moffat, K. Goon, S. Oswald, Prof. F. Guilak  
Center of Regenerative Medicine  
Washington University  
Campus Box 8233, St. Louis, MO 63110, USA  
E-mail: [guilak@wustl.edu](mailto:guilak@wustl.edu)

Dr. K. Moffat, K. Goon, S. Oswald, Prof. F. Guilak  
Shriners Hospitals for Children  
St. Louis, MO 63110, USA

Dr. F. Moutos, Dr. B. Estes, Prof. F. Guilak  
Cytex Therapeutics, Inc.  
Durham, NC 27704, USA

Prof. Xuanhe Zhao  
Department of Mechanical Engineering  
Massachusetts Institute of Technology  
Cambridge, MA 02139, USA

 The ORCID identification number(s) for the author(s) of this article can be found under <https://doi.org/10.1002/mabi.201800140>.

DOI: 10.1002/mabi.201800140

Recent studies have shown that combinations of two or more dissimilar materials that are partially interlaced on a molecular scale, but not covalently linked to each other, can form interpenetrating polymer networks (IPN) with unique and synergistic mechanical properties as compared to standard hydrogels.<sup>[10]</sup> Such dual-network “tough gels” are uniquely suited for this application as they substantially improve the physical properties of the construct by increasing toughness and reducing the coefficient of friction at the articular cartilage interface,<sup>[10c,11]</sup> both of which are critical for clinical translation of engineered tissue constructs. Since this discovery, interest in this technology for cell encapsulation in tissue engineering applications has grown rapidly.<sup>[12]</sup> In general, the combination of polymer networks with different mechanical properties (i.e., a dissipative network and a stretchy network), has resulted in IPN hydrogels that are highly stretchable and tough,<sup>[13]</sup> while at the same time able to support cell encapsulation and viability.<sup>[14]</sup>

However, further work is needed to develop IPNs that have the ability to physically direct stem cell differentiation and tissue growth, while providing enhanced functional mechanical properties to support cartilage regeneration.<sup>[15]</sup> Additionally, several of the more complex properties of collagenous tissues, such as anisotropy, tension–compression nonlinearity, and inhomogeneity are difficult to control with hydrogels, including IPNs. In this respect, the combination of hydrogels with 3D woven scaffolds of poly( $\epsilon$ -caprolactone) (PCL) have been shown to provide biomimetic mechanical properties.<sup>[11b]</sup> Reinforcement of various hydrogels using 3D woven PCL scaffolds has been shown to provide the nonlinear and anisotropic strength of articular cartilage.<sup>[16]</sup> Furthermore, independent of hydrogels, the 3D woven scaffolds have been shown to support MSC viability and chondrogenesis.<sup>[17]</sup> An important challenge in the field has been the development of biomaterial scaffolds that simultaneously support functional biomechanical properties at the macroscopic scale (e.g., compressive modulus, frictional properties), while also providing a controllable local cell “niche” that supports appropriate cell growth and differentiation.

Therefore, the goal of this study was to combine two distinct biocompatible polymer networks—ionically cross-linked agarose with covalently cross-linked PEG-DA—into an IPN hydrogel that can support MSC encapsulation and chondrogenic differentiation while providing enhanced mechanical properties for cartilage replacement. Additionally, as a strategy for cartilage tissue engineering, we developed MSC-seeded fiber-composite constructs by infiltrating this IPN into

3D woven PCL scaffolds to further improve the functional mechanical properties while maintaining a local hydrogel environment for MSCs.

## 2. Results

### 2.1. Mechanical Properties

Swelling behavior differed between the single and dual network hydrogel groups, with or without fiber reinforcement (Figure 1). For each of the hydrogel groups, the swelling ratio did not vary significantly over the 28 days of measurements. Ranging from  $31.0 \pm 1.6$  at Day 1 to  $34.4 \pm 0.8$  at Day 28, the PEG hydrogels consistently exhibited about twice the swelling ratio as the agarose gels ( $14.3 \pm 2.4$  to  $17.2 \pm 1.0$ ), and over three times as much as the IPN gels ( $10.3 \pm 0.3$  to  $10.8 \pm 0.6$ ) for the gel only groups (Figure 1a). The combination of PEG and agarose resulted in a dual network gel (IPN) with a lower and more consistent swelling ratio than each of its individual constituents. Fiber-reinforced (FR) hydrogels displayed markedly lower swelling ratios, which were up to 90% lower than their hydrogel only counterparts (Figure 1b). The swelling ratio for FR-Agarose varied from  $1.4 \pm 0.1$  at Day 1 to  $1.5 \pm 0.1$  at Day 28, FR-PEG varied from  $3.9 \pm 0.1$  to  $3.8 \pm 0.1$ , and FR-IPN varied from  $2.0 \pm 0.1$  to  $2.1 \pm 0.1$ . Moreover, the swelling ratio was much more consistent across all types of FR-hydrogels than for the gel-only groups.

Mechanical properties differed with and without fiber reinforcement, as well as between the single and dual network hydrogel groups (Figure 2). IPN hydrogels demonstrated equilibrium moduli similar to PEG, yet significantly higher than agarose, under uniaxial unconfined compression (Figure 2a). These values remained consistent over the 28-day culture: at Day 1,  $0.01 \pm 0.001$  MPa for agarose,  $0.03 \pm 0.01$  MPa for PEG, and  $0.05 \pm 0.02$  MPa for the IPN. The addition of fiber reinforcement increased the equilibrium moduli of all groups by an order of magnitude at each time point (Figure 2b vs 2a): at Day 1,  $1.19 \pm 0.51$  MPa for FR-Agarose,  $0.39 \pm 0.38$  for FR-PEG, and  $0.34 \pm 0.24$  for FR-IPN. No significant changes over time or between groups were noted for the fiber reinforced groups (Figure 2b). The dynamic moduli of all groups were similar throughout the entire culture period, with the exception of the gel-only agarose group demonstrating an increase from  $0.03 \pm 0.01$  MPa at Day 1 to  $0.05 \pm 0.01$  MPa

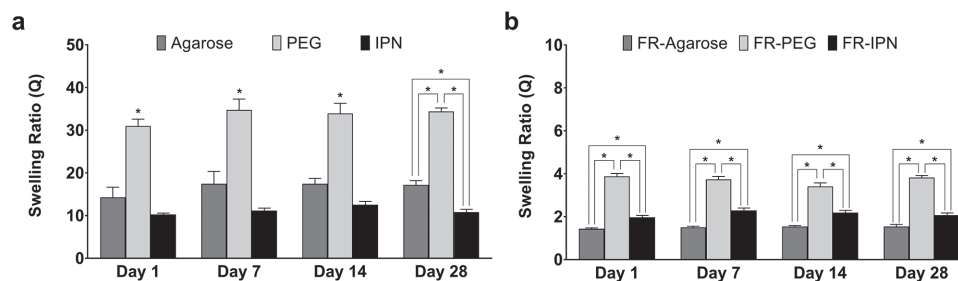


**Figure 1.** Swelling ratios of a) hydrogels and b) fiber-reinforced (FR) hydrogels. Data presented as mean  $\pm$  SEM.  $n = 5$  per group.  $*p < 0.05$  between groups.

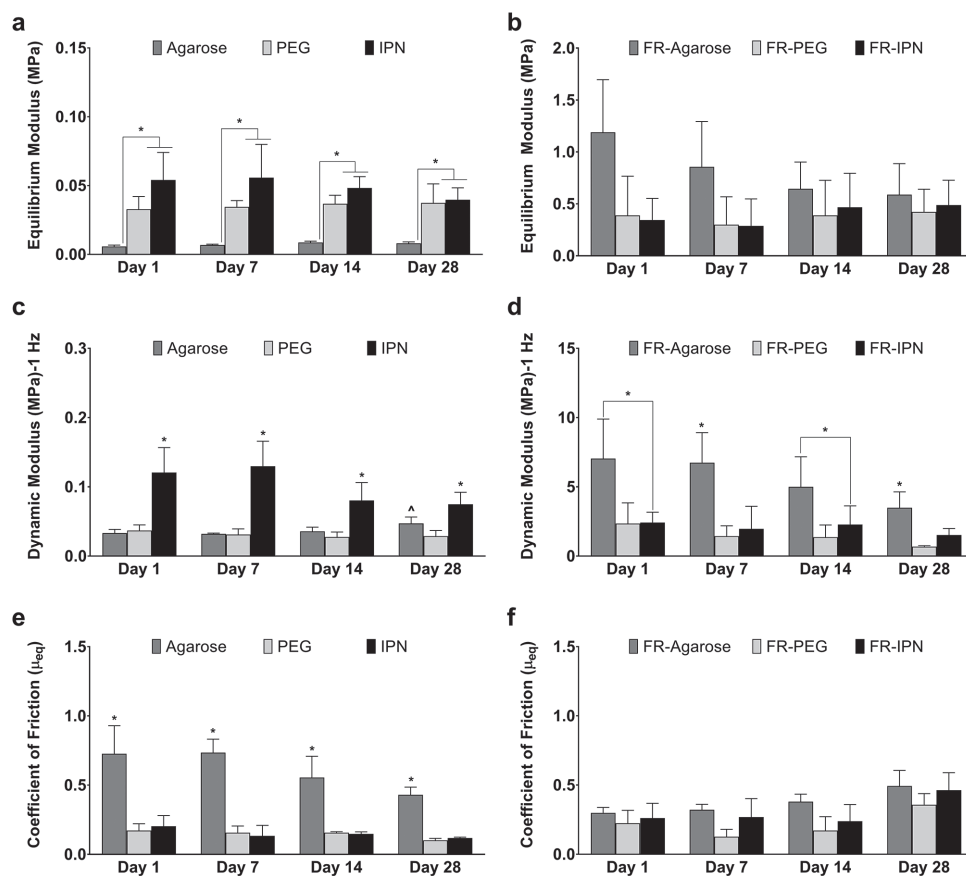


**Figure 2.** Compressive and frictional properties of hydrogels and fiber-reinforced (FR) hydrogels. Equilibrium modulus for a) hydrogels and b) FR-hydrogels. Dynamic modulus at 1.0 Hz for c) hydrogels and d) FR-hydrogels. Coefficient of friction  $\mu_{eq}$  for e) hydrogels and f) FR-hydrogels. Data presented as mean  $\pm$  SEM.  $n = 5$  per group.  $\Delta p < 0.05$  over time,  $*p < 0.05$  between groups.

at Day 28 (Figure 2c). The dynamic moduli of PEG and IPN remained close to the Day 1 levels of  $0.04 \pm 0.01$  MPa and  $0.12 \pm 0.04$  MPa, respectively. Notably, the IPN gel-only group exhibited significantly higher values compared to the gel-only individual component groups at all time points. Similar to the equilibrium compression modulus, the addition of fiber reinforcement increased the dynamic modulus values for all groups at all time points by at least one order of magnitude (Figure 2d vs 2c): at Day 1, the dynamic moduli were  $7.0 \pm 2.8$  MPa for FR-agarose,  $2.3 \pm 1.5$  MPa for FR-PEG, and  $2.4 \pm 0.7$  MPa for FR-IPN. Dynamic moduli at 0.1 and 1.0 Hz were similar within each hydrogel group regardless of rate (data not shown). The values of the friction coefficient,  $\mu_{eq}$ , were significantly higher for the gel-only agarose group ( $0.7 \pm 0.2$ , Day 1) compared to PEG ( $0.2 \pm 0.05$ , Day 1) and IPN ( $0.2 \pm 0.08$ , Day 1) hydrogels (Figure 2e). The addition of fiber reinforcement reduced the coefficient of friction for the FR-agarose group ( $0.3 \pm 0.04$ , Day 1), without significantly increasing the values for the other fiber-reinforced groups, FR-PEG ( $0.2 \pm 0.09$ , Day 1) and FR-IPN ( $0.3 \pm 0.1$ , Day 1) (Figure 2f). Over time, the coefficient of friction remained similar for all groups. The friction coefficient for 3D woven scaffold only, without any hydrogel, also remained similar to that of the FR-agarose at all time points (data not shown).

## 2.2. In Vitro Analysis

Encapsulated hMSCs showed high viability and maintained a spherical phenotype throughout the 28-day culture for all groups (Figure 3). Cells tended to exhibit a clustered arrangement within the PEG hydrogel group. Histological analysis with Safranin-O/Fast Green showed significant positive accumulation of sGAG within all scaffolds, although low staining was observed for collagen (Figure 4). Quantitative matrix synthesis data normalized by DNA content showed that both sGAG and collagen content increased over time for all hydrogel-only groups (Figure 5a,c). At Day 28, sGAG per DNA reached  $11.1 \pm 1.2 \mu\text{g} \mu\text{g}^{-1}$  for agarose,  $11.5 \pm 0.4 \mu\text{g} \mu\text{g}^{-1}$  for PEG, and  $13.4 \pm 1.2 \mu\text{g} \mu\text{g}^{-1}$  for IPN. Collagen content per DNA at Day 28 was  $0.38 \pm 0.07 \mu\text{g} \mu\text{g}^{-1}$  for agarose,  $0.26 \pm 0.05 \mu\text{g} \mu\text{g}^{-1}$  for PEG, and  $0.28 \pm 0.06 \mu\text{g} \mu\text{g}^{-1}$  for IPN. However, sGAG content remained consistent for all FR-hydrogel groups: at Day 28, sGAG per DNA was  $5.9 \pm 1.2 \mu\text{g} \mu\text{g}^{-1}$  in FR-agarose,  $4.7 \pm 1.8 \mu\text{g} \mu\text{g}^{-1}$  in FR-PEG, and  $5.2 \pm 2.7 \mu\text{g} \mu\text{g}^{-1}$  in FR-IPN (Figure 5b). Collagen per DNA trended higher over time in both FR-agarose, reaching  $0.49 \pm 0.04 \mu\text{g} \mu\text{g}^{-1}$  by Day 28, and in FR-IPN, reaching  $0.53 \pm 0.18 \mu\text{g} \mu\text{g}^{-1}$  (Figure 5d). Collagen per DNA remained consistent over time in FR-PEG ( $0.31 \pm 0.08 \mu\text{g} \mu\text{g}^{-1}$  at Day 28).

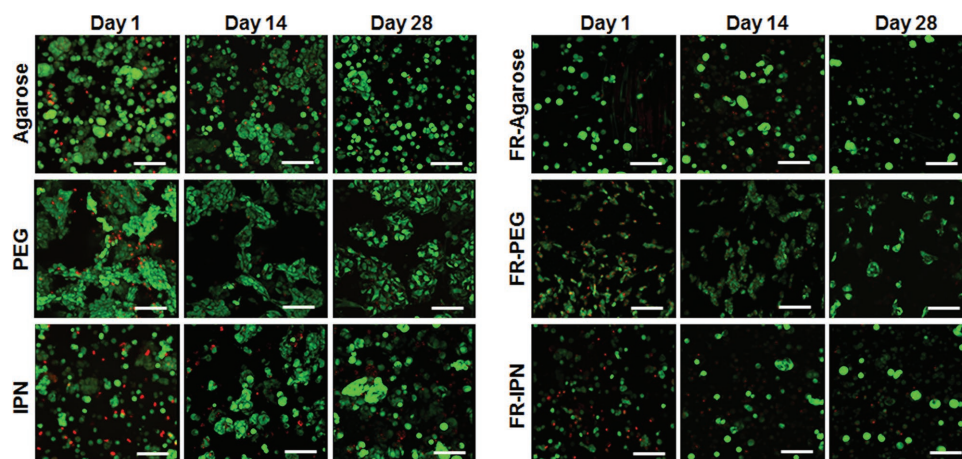


**Figure 3.** Live–dead staining indicating cell viability and morphology over the 28-day timecourse in agarose, PEG and IPN hydrogels as well as fiber-reinforced (FR) hydrogels: FR-agarose, FR-PEG, and FR-IPN (20 $\times$ , scale bar = 100  $\mu$ m).

### 3. Discussion

The findings of this study show that complex hybrid composite materials—consisting of IPN hydrogels reinforced with 3D woven fiber structures—can be used to form scaffolds that possess a locally defined cellular microenvironment, while also forming a macroscopically tunable, functional biomechanical construct. With respect to cellular encapsulation, agarose-PEG IPNs provide for unique synergistic mechanical properties compared to the component polymers (agarose and PEG) alone, while supporting the long-term viability and chondrogenesis of hMSCs. These studies open the possibility for creating hydrogel-based scaffolds that are conducive to

hMSC chondrogenesis but possess tunable biomimetic properties that mimic the local cellular “niche.” While further optimization of IPN properties is likely required, our findings showed significant improvement of various mechanical properties in the IPN hydrogel as compared to the individual hydrogels. When reinforced using a 3D woven fiber structure, the macro-scale compressive properties of the woven construct can provide an even wider range of complex, nonlinear, and anisotropic mechanical properties as compared to those of the infiltrating hydrogels. These results show significant promise in the ability to individually control the local and macro-scale mechanical properties through composite hydrogel and fiber construct modifications.

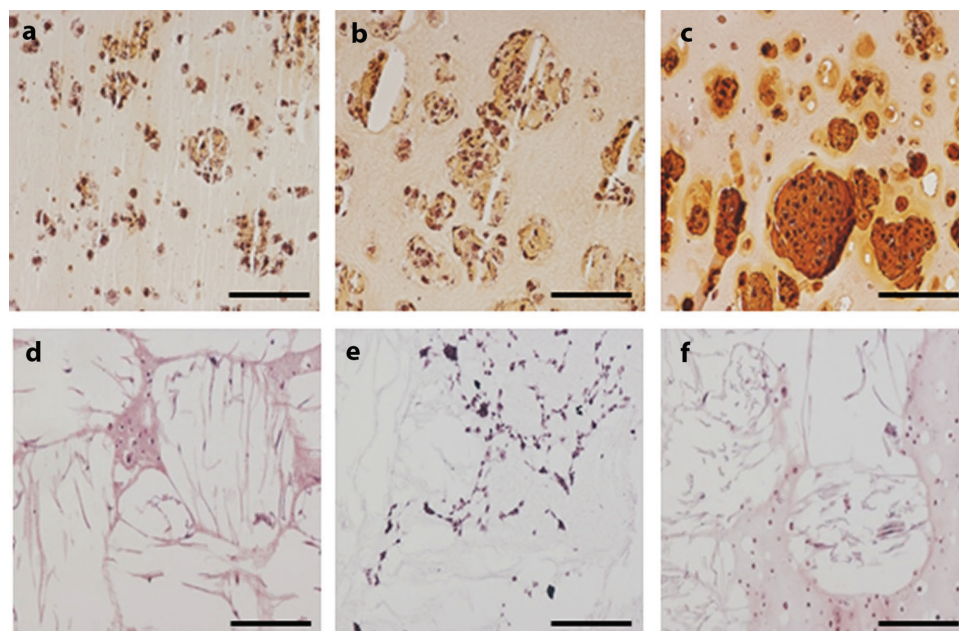


**Figure 4.** Histological analysis of matrix synthesis at Day 28 using Safranin-O/Fast Green (10 $\times$ , scale bar = 200  $\mu$ m, red/orange = sGAG). a) Agarose, b) PEG, c) IPN, d) FR-Agarose, e) FR-PEG, f) FR-IPN.

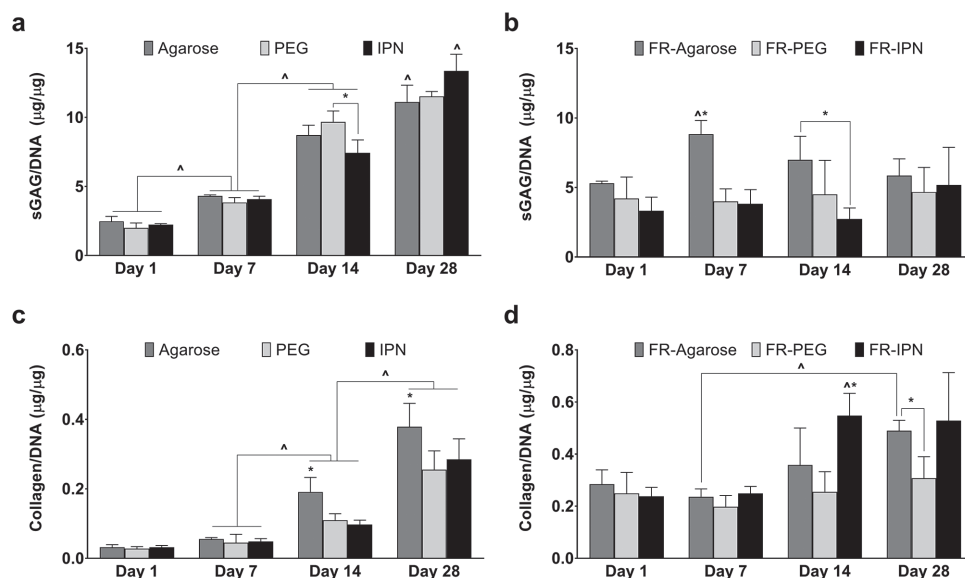


**Figure 5.** Quantitative analysis of matrix synthesis of sGAG per DNA for a) hydrogels and b) fiber reinforced (FR) hydrogels; collagen per DNA for c) hydrogels and d) FR hydrogels, data presented as mean  $\pm$  SEM.  $n = 5$  per group.  $\Delta p < 0.05$  over time,  $*p < 0.05$  between groups.

The IPN chosen for infusion into the 3D woven PCL scaffold was based on a combination of two long-studied biocompatible materials, a brittle agarose network, and a ductile PEG network, previously proven to encapsulate chondrocytes with a high degree of viability while retaining high compressive mechanical properties.<sup>[14b]</sup> Moreover, agarose provides the advantage of a long-established biocompatible material for supporting chondrogenesis in 3D culture.<sup>[18]</sup> In addition to these qualities, PEG also brings the potential for further improvement of chondrogenesis through functionalization.<sup>[19]</sup> Previous work regarding the relative compositions of agarose and PEG in the IPN identified PEG concentration as the most influential factor on IPN mechanical properties, with PEG molecular weight as a significant contributor to improved failure properties.<sup>[20]</sup> To that end, agarose was maintained at the previously used 2% concentration,<sup>[14b]</sup> and variations in PEG concentration as well as molecular weight were tested. The final concentration (20% w/v) and molecular weight (10 kDa) were selected based on optimal equilibrium moduli (Figure S1, Supporting Information). It should also be noted that at 5% w/v PEG-DA, the unique synergistic effect of the agarose-PEG IPN is not realized. Fluorescence imaging was used to verify that the distribution of this agarose-PEG IPN combination matched previously characterized structure, showing complete infiltration of the IPN into the 3D woven PCL (Figure S2, Supporting Information).<sup>[21]</sup> Live-dead cell microscopy (Figure 3) and histology (Figure 4), illustrating the distribution of cells throughout the composite structure, further confirmed the previously established composite micro-structure of hydrogel infused into 3D woven scaffold.<sup>[16a,c]</sup>

The combination of agarose and PEG into the IPN gel allowed for a synergistic control over the mechanical properties and shape retention of the scaffold, with a further level of control exerted by the embedded 3D woven fiber reinforcement. The measured swelling ratios for IPNs were significantly

lower than that of PEG-only hydrogels and further decreased by an order of magnitude for the fiber-reinforced hydrogels. It should be noted that the swelling ratio is related to cross-linking density: higher swelling ratios indicate lower cross-linking density.<sup>[8b]</sup> MSCs have been shown to produce more uniform ECM in PEG hydrogels with swelling ratios similar to those of the gel-only constructs, around 15,<sup>[22]</sup> than in hydrogels with lower swelling ratios, such as those of the fiber-reinforced hydrogels. This study demonstrated high cell viability under all conditions, but further optimization of swelling ratios may allow for improved chondrogenesis and matrix accumulation through increased diffusion in the hydrogel, shown to be limited in the fiber-reinforced gels in the current study. The increase in GAG content over time indicates that the IPN gels can support differentiating MSCs with chondrogenesis at a level comparable to the individual agarose and PEG gels.<sup>[12e,23]</sup> While the fiber-reinforced gels did not show an increase over time in GAG levels, some increases were noted in collagen levels and consistent levels of both were maintained. The high molecular weight of the PEG in the IPN, optimized for mechanical strength, may also have had a limiting effect on the GAG content.<sup>[20]</sup> The increase in collagen content over time for the gel-only samples indicates that the IPN gels can support robust tissue synthesis at a level comparable to the individual PEG gels. In previous studies examining MSC behavior in semi-IPN poly(vinyl alcohol) and poly(caprolactone) scaffolds, the total collagen content at 28 days was comparable to the levels in our study in the first week.<sup>[23a]</sup> Although the individual agarose gels exhibited higher levels of collagen production than the IPN hydrogels, the overall improvement in mechanical properties for the IPN hydrogels outweighs any minor loss in collagen production. Furthermore, large swelling ratios may confound the ability to accurately produce patient-specific hydrogel implants that require precise control of final size and shape. By embedding a 3D woven fiber into the hydrogel networks, we were

able to greatly reduce their swelling behavior. In this case, the embedded fibers, which are markedly more stiff than the gel components, acted to reinforce the hydrogels and restrict their ability to freely swell and expand,<sup>[11b]</sup> allowing for prescribed definition of the final dimensions of the tissue constructs.

In addition to the control over swelling ratios, the IPN allows significant additional control of the mechanical properties over agarose and PEG individually, and scaffold fiber-reinforcement can provide further control of the macroscopic mechanical properties to mimic those of native articular cartilage. In fiber-reinforced IPN constructs, both the equilibrium modulus and the dynamic modulus were further increased by an order of magnitude. In most tissue engineering approaches, the effect of tissue growth is offset by the effect of biomaterial degradation of the scaffold, which tends to diminish mechanical properties over time.<sup>[12b]</sup> In the present study, these properties remained consistent throughout the culture period, indicating that the fiber-reinforced gel maintains structural integrity over time.<sup>[14b,16c]</sup> The one exception to the steady level of the moduli was the increase in dynamic modulus of Agarose-only at Day 28. This increase corresponds with cell matrix deposition indicated by the highest level of collagen measured in the Agarose-only group at Day 28. Both the equilibrium modulus and the dynamic modulus achieved levels on the order of those found for native cartilage explants, and furthermore, these constructs exhibit frictional properties comparable to that of articular cartilage.<sup>[11b]</sup> Although the coefficient of friction did increase with the addition of fiber reinforcement for both PEG and IPN samples, levels remained close to previously reported coefficients of friction for cartilage.<sup>[16c]</sup> A slight increase in coefficient of friction is expected with the addition of the scaffold.<sup>[11b]</sup> The one exception to this trend occurred with the agarose-only gels: the coefficient of friction for agarose-only was already so high that infusion of agarose into the fiber-reinforced scaffold served to lower the coefficient of friction for FR-agarose. As with the other mechanical properties, the coefficient of friction maintained a consistent level over time, further indicating the structural integrity of the fiber-reinforced gels.

## 4. Conclusions

Taken together, our findings indicate that the combination of agarose and PEG into an IPN hydrogel can provide the ability to modulate macro-scale structural properties, while supporting MSC viability and differentiation in the cellular microenvironment. Fiber reinforcement can further improve the macroscopic mechanical properties to a biomimetic level. The ability to tailor the anisotropy, nonlinearity, and viscoelasticity of the fiber scaffold,<sup>[21]</sup> in combination with a diverse array of hydrogels,<sup>[8a,9b,c,11b,12b,d]</sup> provides a paradigm for development of complex scaffolds with tailored mechanical properties at multiple scales.

## 5. Experimental Section

**Agarose Hydrogel Synthesis:** Agarose hydrogels (2% w/v, Type VII, Sigma-Aldrich, St. Louis, MO) were fabricated via a thermo-reversible process that resulted in physically cross-linked hydrogels. Briefly, agarose powder (0.4 g) was mixed into phosphate buffered saline (10 mL, PBS, Sigma-Aldrich) and autoclaved for 30 min. Agarose was allowed to

cool to 39 °C and was then combined with cell-culture media to yield an agarose solution (2% w/v). The agarose solution was then pipetted into cylindrical silicone molds (6 mm diameter, 2 mm height). The gels were allowed to cool at room temperature for 30 min prior to removal from the mold. Agarose discs were then added to a reservoir of PBS and allowed to equilibrate for 4 h.

**PEG-DA Hydrogel Synthesis:** PEG-DA hydrogels were fabricated by covalently cross-linking poly(ethylene) glycol-diacrylate (PEG-DA) (20% w/v, 10 kDa, Creative PEG Works, Chapel Hill, NC) via photopolymerization in the presence of a photoinitiator (0.1% w/v Irgacure 2959, Ciba). Irgacure 2959 powder was added to autoclaved PBS to create a working solution (1% w/v), which was subsequently added to a PEG-DA solution (20% w/v, 20 mg PEG-DA, 90  $\mu$ L sterile PBS, 10  $\mu$ L photoinitiator working solution 1% w/v). The PEG-DA solution (20% w/v) was pipetted into a custom polypropylene mold (6 mm diameter, 2 mm height) and exposed to UV light (365 nm wavelength) for 10 min. Following photopolymerization, the PEG-DA hydrogel discs were removed from the mold and allowed to equilibrate in a reservoir of PBS for 4 h.

**Agarose-PEG Interpenetrating Polymer Network Hydrogel Synthesis:** Agarose-PEG IPN hydrogels were fabricated by first casting an agarose gel (as previously described), which was subsequently immersed in a solution of PEG-DA (20% w/v, 10 kDa) containing the photoinitiator for 3 h at 37 °C. The agarose-PEG gel was then exposed to UV light (365 nm wavelength) for 5 min to cross-link the PEG-DA.

**Fiber-Reinforced Hydrogel Production:** Fiber-reinforced (FR) hydrogels were produced using a previously described vacuum-assisted infusion technique to infuse agarose, PEG, or IPN gels into a 3D orthogonally woven poly( $\epsilon$ -caprolactone) (PCL) scaffold (0.8 mm thick).<sup>[16c]</sup> Immediately after infusion, the gels were cross-linked, as previously described, to form the final composite structures (Figure 6). The PEG-DA molecular weight and concentration were selected by comparing the equilibrium modulus for FR-PEG gels and FR-IPN gels: using 20% w/v PEG-DA at either 5 or 10 kDa, and using 10 kDa MW PEG-DA at either 5% w/v or 20% w/v (Figure S1, Supporting Information). With the higher resulting equilibrium modulus in the FR-IPN (0.28  $\pm$  0.01 MPa vs 0.18  $\pm$  0.01 MPa), the molecular weight of 10 kDa PEG-DA was selected. Similarly, with the higher resulting equilibrium modulus in the FR-IPN (0.28  $\pm$  0.01 MPa vs 0.02  $\pm$  0.01 MPa), the concentration of 20% w/v PEG-DA was selected.

**Human Mesenchymal Stem Cells:** Human mesenchymal stem cells (hMSCs) were derived from bone marrow aspirates obtained from healthy adults. Informed consent was obtained, and an Institutional Review Board-approved aspiration procedure was used. Briefly, the bone marrow sample was washed with Dulbecco's modified Eagle's medium (DMEM-LG, Gibco, Waltham, MA) supplemented with fetal bovine serum (FBS, 10%) from a selected lot. The sample was centrifuged (460 g) on a preformed Percoll density gradient (1.073 g mL<sup>-1</sup>) to isolate the mononucleated cells. These cells were resuspended in serum-supplemented medium and seeded in 10 cm diameter plates (density 1.8  $\times$  10<sup>5</sup> cells cm<sup>-2</sup>). Nonadherent cells were removed after 4 days by changing the medium. For the remainder of the cell expansion phase, the medium was additionally supplemented with recombinant human

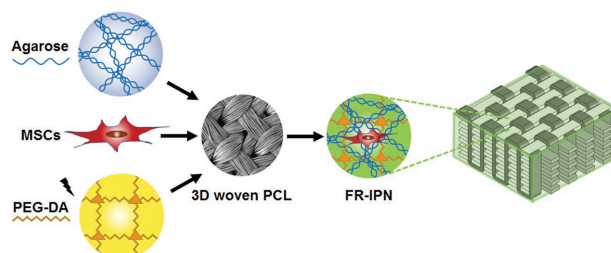


**Figure 6.** Schematic of the process for forming cellularized, fiber-reinforced IPNs by combining MSC-seeded agarose and PEG-DA infiltrated into a 3D woven PCL scaffold.

fibroblast growth factor-basic (1 ng mL<sup>-1</sup>, rhFGF-2, Peprotech, Rocky Hill, NJ), and was replaced twice per week. The primary culture was trypsinized after approximately two weeks, and then cryopreserved using Gibco freezing medium.

**Tissue Engineered Constructs:** hMSCs were thawed and plated (density 5500 cells cm<sup>-2</sup>), and cultured in supplemented medium (DMEM-LG, Gibco, supplemented with 10% FBS, 1 ng mL<sup>-1</sup> rhFGF-2, and 1% penicillin-streptomycin-fungizone). Medium was completely replaced every 3 days until cells reached 80% confluence, after which they were passaged and replated. After the fourth passage (P4), cells were encapsulated into hydrogels (density 5 × 10<sup>6</sup> cells mL<sup>-1</sup>) immediately prior to molding and cross-linking. After molding, cell-loaded discs were transferred to 24 well ultra-low attachment plates (Corning, NY) and cultured in chondrogenic medium (1 mL). Chondrogenic culture medium consisted of DMEM-HG supplemented with ITS+ premix (1%, Collaborative Biomedical, Becton Dickinson, Bedford, MA), dexamethasone (100 nM, Sigma), penicillin (100 U mL<sup>-1</sup>), streptomycin (100 U mL<sup>-1</sup>), L-ascorbic acid 2-phosphate (37.5 mg mL<sup>-1</sup>), and recombinant human transforming growth factor beta (1 ng mL<sup>-1</sup>, TGF-β3, R&D Systems, Minneapolis, MN). Medium was completely replaced for all groups every 2–3 days and constructs were harvested at days 1, 7, 14, and 28. Samples of each group per time point included: *n* = 5 for each type of mechanical testing, *n* = 3 to evaluate cell viability and morphology, *n* = 5 for biochemical analysis, and *n* = 3 for histology.

**Mechanical Testing—Swelling Ratio:** For *n* = 5 samples of each type of hydrogel, the volumetric swelling ratio (*Q*) of each hydrogel was quantified by measuring the equilibrium wet and dry weights, and calculating the ratio of the difference in weights to the original dry weight.

**Compressive Mechanical Testing:** At each time point, samples of 3 mm diameter were cored from the central region of each 6 mm diameter construct and subjected to unconfined compression. An ELF 3200 Series precision controlled materials testing system (TA Instruments, New Castle, DE) was used to perform stress relaxation experiments in an unconfined compression configuration. Strains of  $\epsilon = 0.04, 0.08, 0.12$  were applied to the specimens after equilibration of a tare load (4 gf). Strain steps were held constant for 1500 s, allowing the scaffolds to relax to an equilibrium level. Equilibrium Young's modulus (*E*) was determined by performing linear regression on the resulting equilibrium stress–strain plot. The dynamic moduli of the samples were determined as previously reported.<sup>[24]</sup> After equilibration of a tare load (4 gf), test samples were cyclically loaded from 0 to 20% strain levels. Samples were tested at both 0.1 and 1 Hz, with 1000 s of relaxation time between tests.

**Frictional Properties:** At each time point, samples of 3 mm diameter were cored from the central region of each 6 mm diameter construct and subjected to frictional mechanical testing. The equilibrium friction coefficient,  $\mu_{eq}$ , was determined using a shear friction testing method.<sup>[25]</sup> Briefly, samples were fixed in a PBS bath and subjected to a 10% compressive tare strain using a stainless steel platen. After the resulting stress equilibrated, a series of sequential angular velocities,  $\omega = 0.01, 0.1, 1, \text{ and } 10 \text{ rad s}^{-1}$ , were applied for a duration of 120 s each. Normal force, *N*, and frictional torque, *T*, were recorded during each step. The average frictional force, *F*, was calculated from the ratio of the measured frictional torque and the radius of the specimen, and used for calculating the equilibrium friction coefficient,  $\mu_{eq}$ , from the ratio of *F* to *N*. The coefficient of friction,  $\mu_{eq}$ , was reported at 10 rad s<sup>-1</sup>.

**Cell Viability and Morphology:** Cell viability and attachment morphology were evaluated using Live-Dead staining (Invitrogen, Waltham, MA). Constructs were rinsed twice with PBS and stained following the manufacturers' suggested protocol. The samples were imaged using confocal laser scanning microscopy (Zeiss LSM 510) at wavelengths of 488 and 568 nm.

**Histology:** Constructs were fixed overnight at 4 °C in a solution containing paraformaldehyde (4%) in a sodium cacodylate buffer (0.100 M, pH 7.4), dehydrated in graded ethanol steps, embedded in paraffin wax, cut into cross sections (10 mm thick) using a Reichart–Jung microtome, and mounted on SuperFrost microscope slides (Microm International AG, Volketswil, Switzerland). Samples were

stained for sulfated glycosaminoglycans (GAGs) and the production of a collagenous matrix using a safranin-O solution (0.1% aqueous) and fast green solution (0.02%), respectively, while also using hematoxylin as a nucleus counterstain. Human osteochondral tissue was used as a positive control.

**Biochemical Analysis:** Samples were digested in papain solution (1 mL, 125 μg mg<sup>-1</sup> papain, 0.1 M sodium phosphate buffer, 0.005 M cysteine hydrochloride, and 0.005 M EDTA, pH 6.5) at 60 °C for 15 h. Total DNA content was determined fluorometrically using the PicoGreen double-stranded DNA (dsDNA) assay (Molecular Probes, Eugene, OR). Sulfated GAG content was measured using the dimethylmethylene blue assay (DMB) as previously described.<sup>[26]</sup> Hydroxyproline (OHP) was used to determine total collagen content of the cultured constructs. Briefly, sample digest was acid hydrolyzed and reacted with 4-Dimethylaminobenzaldehyde and chloramine-T to measure OHP content per construct. Total collagen was then determined using 0.134 as the ratio of OHP to collagen. GAG content and collagen content were normalized to DNA content.

## Statistical Analysis

Analysis of variance (ANOVA) with Tukey–Kramer HSD post hoc test was performed to compare the results of mechanical and biochemical tests for each construct between time points ( $\alpha = 0.05$ ).

## Supporting Information

Supporting Information is available from the Wiley Online Library or from the author.

## Acknowledgements

This work was supported in part by NIH grants AR50245, AR48852, AG15768, AR48182, AG46927, the Washington University Musculoskeletal Research Center (NIH P30 AR057235), the Collaborative Research Center, AO Foundation, Davos, Switzerland, the Arthritis Foundation, and the Nancy Taylor Foundation for Chronic Diseases.

## Conflict of Interest

Dr. F. Guilak, Dr. F. Moutos, and Dr. B. Estes are paid employees of Cytek Therapeutics.

## Keywords

chondrocyte, fiber-reinforced, MSC, osteoarthritis, tough gel

Received: April 17, 2018

Revised: June 21, 2018

Published online: July 24, 2018

[1] B. Johnstone, M. Alini, M. Cucchiari, G. R. Dodge, D. Eglon, F. Guilak, H. Madry, A. Mata, R. L. Mauack, C. E. Semino, M. J. Stoddart, *Eur. Cell. Mater.* **2013**, 25, 248.

[2] a) M. Manfredini, F. Zerbinati, A. Gildone, R. Faccini, *Acta Orthop. Belg.* **2007**, 73, 207; b) G. Knutsen, J. O. Drogset, L. Engebretsen, T. Grontvedt, V. Isaksen, T. C. Ludvigsen, S. Roberts, E. Solheim, T. Strand, O. Johansen, *J. Bone Joint Surg. Am.* **2007**, 89, 2105.

- [3] J. J. Wood, M. A. Malek, F. J. Frassica, J. A. Polder, A. K. Mohan, E. T. Bloom, M. M. Braun, T. R. Cote, *J. Bone Joint Surg. Am.* **2006**, *88*, 503.
- [4] P. Niemeyer, J. M. Pestka, P. C. Kreuz, C. Erggelet, H. Schmal, N. P. Suedkamp, M. Steinwachs, *Am. J Sports Med.* **2008**, *36*, 2091.
- [5] a) F. Guilak, B. T. Estes, B. O. Diekman, F. T. Moutos, J. M. Gimble, *Clin. Orthop. Relat. Res.* **2010**, *468*, 2530; b) A. H. Huang, M. J. Farrell, R. L. Mauck, *J. Biomech.* **2010**, *43*, 128; c) J. A. Anderson, D. Little, A. P. Toth, C. T. Moorman, B. S. Tucker, M. G. Ciccotti, F. Guilak, *Am. J. Sports Med.* **2014**, *42*, 2253; d) L. F. Mellor, M. Mohiti-Asli, J. Williams, A. Kannan, M. R. Dent, F. Guilak, E. G. Lobo, *Tissue Eng. Part A* **2015**, *21*, 2323; e) Q. O. Tang, C. F. Carasco, Z. Gamie, N. Korres, A. Mantalaris, E. Tsiroidis, *Expert Opin. Biol. Ther.* **2012**, *12*, 1361; f) T. Gonzalez-Fernandez, E. G. Tierney, G. M. Cunniffe, F. J. O'Brien, D. J. Kelly, *Tissue Eng. Part A* **2016**, *22*, 776.
- [6] J. L. Drury, D. J. Mooney, *Biomaterials* **2003**, *24*, 4337.
- [7] a) G. Filardo, E. Kon, A. Roffi, A. Di Martino, M. Marcacci, *Arthroscopy* **2013**, *29*, 174; b) S. Fischer, A. Kisser, *J. Orthop.* **2016**, *13*, 246; c) E. Kon, A. Roffi, G. Filardo, G. Tesei, M. Marcacci, *Arthroscopy* **2015**, *31*, 767; d) J. Liao, K. Shi, Q. Ding, Y. Qu, F. Luo, Z. Qian, *J Biomed. Nanotechnol.* **2014**, *10*, 3085; e) S. Nuernberger, N. Cyran, C. Albrecht, H. Redl, V. Vecsei, S. Marlovits, *Biomaterials* **2011**, *32*, 1032.
- [8] a) J. Yang, Y. Shrike Zhang, K. Yue, A. Khademhosseini, *Acta Biomater.* **2017**, <https://doi.org/10.1016/j.actbio.2017.01.036>; b) K. L. Spiller, S. A. Maher, A. M. Lowman, *Tissue Eng. Part B Rev.* **2011**, *17*, 281.
- [9] a) C. T. Hung, R. L. Mauck, C. C. Wang, E. G. Lima, G. A. Ateshian, *Ann. Biomed. Eng.* **2004**, *32*, 35; b) B. V. Sridhar, E. A. Dailing, J. L. Brock, J. W. Stansbury, M. A. Randolph, K. S. Anseth, *Regen. Eng. Transl. Med.* **2015**, *1*, 11; c) A. J. Neumann, T. Quinn, S. J. Bryant, *Acta Biomater.* **2016**, *39*, 1.
- [10] a) J. P. Gong, Y. Katsuyama, T. Kurokawa, Y. Osada, *Adv. Mater.* **2003**, *15*, 1155; b) K. Yasuda, J. P. Gong, Y. Katsuyama, A. Nakayama, Y. Tanabe, E. Kondo, M. Ueno, Y. Osada, *Biomaterials* **2005**, *26*, 4468; c) J. Y. Sun, X. Zhao, W. R. Illeperuma, O. Chaudhuri, K. H. Oh, D. J. Mooney, J. J. Vlassak, Z. Suo, *Nature* **2012**, *489*, 133.
- [11] a) H. Bodugoz-Senturk, C. E. Macias, J. H. Kung, O. K. Muratoglu, *Biomaterials* **2009**, *30*, 589; b) I. C. Liao, F. T. Moutos, B. T. Estes, X. Zhao, F. Guilak, *Adv. Funct. Mater.* **2013**, *23*, 5833; c) S. Lin, C. Cao, Q. Wang, M. Gonzalez, J. E. Dolbow, X. Zhao, *Soft Matter* **2014**, *10*, 7519.
- [12] a) K. Yasuda, N. Kitamura, J. P. Gong, K. Arakaki, H. J. Kwon, S. Onodera, Y. M. Chen, T. Kurokawa, F. Kanaya, Y. Ohmiya, Y. Osada, *Macromol. Biosci.* **2009**, *9*, 307; b) G. C. Ingavle, S. H. Gehrke, M. S. Detamore, *Biomaterials* **2014**, *35*, 3558; c) L. C. Yin, X. Zhao, L. M. Cui, J. Y. Ding, M. He, C. Tang, C. H. Yin, *Food Chem. Toxicol.* **2009**, *47*, 1139; d) S. C. Skaalure, S. O. Dimson, A. M. Pennington, S. J. Bryant, *Acta Biomater.* **2014**, *10*, 3409; e) A. N. Buxton, J. Zhu, R. Marchant, J. L. West, J. U. Yoo, B. Johnstone, *Tissue Eng* **2007**, *13*, 2549; f) L. Recha-Sancho, F. T. Moutos, J. Abella, F. Guilak, C. E. Semino, *Materials (Basel)* **2016**, *9*, 472; g) J. M. Gimble, F. T. Guilak, M. E. Nuttall, S. Satishkumar, M. E. Vidal, B. A.E. Bunnell, *Transfus. Med. Hemother.* **2008**, *35*, 228–238.
- [13] X. Zhao, *Soft Matter* **2014**, *10*, 672.
- [14] a) S. Hong, D. Sycks, H. F. Chan, S. Lin, G. P. Lopez, F. Guilak, K. W. Leong, X. Zhao, *Adv. Mater.* **2015**, *27*, 4035; b) B. J. DeKosky, N. H. Dormer, G. C. Ingavle, C. H. Roatch, J. Lomakin, M. S. Detamore, S. H. Gehrke, *Tissue Engineering. Part C Methods* **2010**, *16*, 1533; c) M. D. Brigham, A. Bick, E. Lo, A. Bendali, J. A. Burdick, A. Khademhosseini, *Tissue Eng Part A* **2009**, *15*, 1645.
- [15] M. C. Darnell, J. Y. Sun, M. Mehta, C. Johnson, P. R. Arany, Z. Suo, D. J. Mooney, *Biomaterials* **2013**, *34*, 8042.
- [16] a) F. T. Moutos, B. T. Estes, F. Guilak, *Macromol Biosci* **2010**, *10*, 1355; b) F. T. Moutos, F. Guilak, *Biorheology* **2008**, *45*, 501; c) F. T. Moutos, F. Guilak, *Tissue Eng. Part A* **2010**, *16*, 1291.
- [17] a) P. K. Valonen, F. T. Moutos, A. Kusanagi, M. G. Moretti, B. O. Diekman, J. F. Welter, A. I. Caplan, F. Guilak, L. E. Freed, *Biomaterials* **2010**, *31*, 2193; b) J. M. Brunger, N. P. Huynh, C. M. Guenther, P. Perez-Pinera, F. T. Moutos, J. Sanchez-Adams, C. A. Gersbach, F. Guilak, *Proc. Natl. Acad. Sci. U. S. A.* **2014**, *111*, E798; c) K. A. Glass, J. M. Link, J. M. Brunger, F. T. Moutos, C. A. Gersbach, F. Guilak, *Biomaterials* **2014**, *35*, 5921.
- [18] a) R. L. Mauck, X. Yuan, R. S. Tuan, Osteoarthritis and cartilage/OARS, Osteoarthritis Research Society **2006**, *14*, 179; b) P. D. Benya, J. D. Shaffer, *Cell* **1982**, *30*, 215.
- [19] G. C. Ingavle, N. H. Dormer, S. H. Gehrke, M. S. Detamore, *J. Mater. Sci. Mater. Med.* **2012**, *23*, 157.
- [20] D. A. Rennerfeldt, A. N. Renth, Z. Talata, S. H. Gehrke, M. S. Detamore, *Biomaterials* **2013**, *34*, 8241.
- [21] F. T. Moutos, L. E. Freed, F. Guilak, *Nat. Mater.* **2007**, *6*, 162.
- [22] H. Park, X. Guo, J. S. Temenoff, Y. Tabata, A. I. Caplan, F. K. Kasper, A. G. Mikos, *Biomacromolecules* **2009**, *10*, 541.
- [23] a) N. Mohan, P. D. Nair, Y. Tabata, *J. Biomed. Mater. Res. A* **2010**, *94*, 146; b) N. Mohan, P. D. Nair, *Tissue Eng Part A* **2010**, *16*, 373; c) R. Tsaryk, A. Gloria, T. Russo, L. Anspach, R. De Santis, S. Ghanaati, R. E. Unger, L. Ambrosio, C. J. Kirkpatrick, *Acta Biomater.* **2015**, *20*, 10.
- [24] S. Park, C. T. Hung, G. A. Ateshian, *Osteoarthr. Cartil.* **2004**, *12*, 65.
- [25] H. Q. Wang, G. A. Ateshian, *J. Biomech.* **1997**, *30*, 771.
- [26] B. T. Estes, B. O. Diekman, J. M. Gimble, F. Guilak, *Nat. Protoc.* **2010**, *5*, 1294.